

## New approach based on continuum damage mechanics with simple parameter identification to fretting fatigue life prediction\*

Fei SHEN, Weiping HU<sup>†</sup>, Qingchun MENG

Institute of Solid Mechanics, School of Aeronautics Science and Engineering,  
Beihang University, Beijing 100191, China

**Abstract** A new continuum damage mechanics model for fretting fatigue life prediction is established. In this model, the damage evolution rate is described by two kinds of quantities. One is associated with the cyclic stress characteristics obtained by the finite element (FE) analysis, and the other is associated with the material fatigue property identified from the fatigue test data of standard specimens. The wear is modeled by the energy wear law to simulate the contact geometry evolution. A two-dimensional (2D) plane strain FE implementation of the damage mechanics model and the energy wear model is presented in the platform of ABAQUS to simulate the evolutions of the fatigue damage and the wear scar. The effect of the specimen thickness is also investigated. The predicted results of the crack initiation site and the fretting fatigue life agree well with available experimental data. Comparisons are made with the critical plane Smith-Watson-Topper (SWT) method.

**Key words** fretting fatigue, continuum damage mechanics, wear, fatigue life, finite element (FE) analysis

**Chinese Library Classification** O346.2, V215.5

**2010 Mathematics Subject Classification** 74R99

### 1 Introduction

Fretting is a contact damage process, arising from the surface micro-slip associated with the small scale oscillatory motion of clamped structural members. Fretting is recognized primarily as a surface damage phenomenon. It is usually used to describe the situations where the contact and micro-slip weaken the fatigue performance of the contacting components. Due to fretting, the component fatigue life decreases drastically when it is compared with the plain fatigue in the case where the wear is insignificant. Many real-life service components have the potential to experience fretting damage, e.g., grips used in plain fatigue tests, bolted and riveted connections, and blade-disk attachments in gas and steam turbines<sup>[1]</sup>.

Fretting fatigue can be divided into two main phases, i.e., crack initiation and crack propagation. Many different methods have been adopted to recognize and investigate the fretting fatigue crack initiation behaviors<sup>[1–7]</sup>. Hills and Nowell<sup>[1]</sup>, Nowell et al.<sup>[2]</sup>, and Nishioka and Hirakawa<sup>[3]</sup> investigated the fretting fatigue problems experimentally. Szolwinski and Farris<sup>[4]</sup>, Lykins et al.<sup>[5]</sup>, Araujo and Nowell<sup>[6]</sup>, and Naboulsi and Mall<sup>[7]</sup> investigated the problem theoretically.

---

\* Received Aug. 21, 2014 / Revised Jun. 3, 2015

Project supported by the National Natural Science Foundation of China (No. 11002010)

<sup>†</sup> Corresponding author, E-mail: huweiping@buaa.edu.cn

Nishioka and Hirakawa<sup>[3]</sup> proposed the cylindrical pads clamped against a flat specimen. Szolwinski and Farris<sup>[4]</sup> extended the multi-axial fatigue theory (the critical plane Smith-Watson-Topper (SWT) parameter) combining the strain-life ideas with a maximum normal stress to predict both the crack initiation site and the fretting fatigue life. Lykins et al.<sup>[5]</sup> evaluated many parameters for predicting the fretting fatigue crack initiation, e.g., the strain based fatigue parameters (the strain-life parameter, the maximum strain corrected for the strain ratio effects, and the maximum principle strain corrected for the principle strain ratio effects), the critical plane based fatigue parameters (the critical plane SWT parameter and the Fatemi-Socie (FS) parameter), and the Ruiz parameters. Araujo and Nowell<sup>[6]</sup> revealed that there was a contact size effect on the fretting fatigue life and the critical plane models resulted in the conservative predictions, and proposed an averaging method on the critical plane model. Naboulsi and Mall<sup>[7]</sup> also proposed an averaging method on the critical plane models.

Besides these multi-axial fatigue approaches, the damage mechanics approaches have also been widely used to solve the fretting fatigue problems<sup>[8-9]</sup>. Zhang et al.<sup>[8]</sup> developed a coupled damage mechanics approach in conjunction with the finite element analysis (FEA) to predict the fretting fatigue life. Hojjati-Talemi and Abdel-Wahab<sup>[9]</sup> used an uncoupled damage evolution approach to predict the fretting fatigue crack initiation lifetime under various loading conditions. The main advantage of the coupled damage mechanics approach is that the coupling relation between the damage field and the stress field can be considered.

The wear effect on the contact surface and sub-surface contact variables, such as the contact pressure, the slip, the stresses, and the critical plane parameters, has been widely studied. McColl et al.<sup>[10]</sup> developed a finite element (FE) simulation for the fretting wear based on a modified Archard wear model. Madge et al.<sup>[11-12]</sup> combined the modified Archard wear model with the critical plane method to evaluate the fretting wear effect on the fretting fatigue life. Zhang et al.<sup>[13]</sup> predicted a fretting performance of two different contact geometries with the energy wear model proposed by Fouvry et al.<sup>[14]</sup>. It has been shown that the energy wear model is superior to the Archard-based model, since a single wear coefficient can be used across a wide range of fretting load-stroke combinations, specifically including both partial slip and gross sliding regimes.

This paper is concerned with the fretting fatigue crack initiation behavior. A new continuum damage mechanics model is established for the fretting fatigue life prediction. In this model, the material parameters in the damage evolution equation can be identified in a simple way by only using the plain fatigue experimental data. The wear is modeled by the energy wear law to simulate the evolution of the contact geometry. The fretting fatigue life is predicted in an FE implementation of the damage mechanics model and the energy wear model in the platform of ABAQUS, where the effects of the damage and wear are considered. The calculated results are validated with the experimental data. Comparisons are also made with the critical plane SWT method.

## 2 Theoretical models

### 2.1 Continuum damage model

Lemaitre and Chaboche<sup>[15]</sup> have presented some fundamental concepts in damage mechanics. The damage in the mechanical sense for solid materials is the creation and growth of microvoids or micro-cracks, which are discontinuous at micro-scale but considered to be continuous at macro-scale. A damage variable is introduced to define the effective surface of the microvoids and micro-cracks in the representative volume element (RVE). The evolution law of the damage variable is formulated in the framework of thermodynamics. Macro-cracks will occur once the accumulated damage reaches a critical value. At that time, the mechanical property of the RVE will be fully degenerated, and its carrying capacity will lose entirely.

### 2.1.1 Damage evolution law

The deterioration of materials will result in the stiffness reduction of the RVE<sup>[16]</sup>. Considering the isotropic damage in isotropic elastic materials, we can define the damage variable as follows:

$$D = \frac{E - E_D}{E}, \quad (1)$$

where  $E$  is Young's modulus of the virgin material, and  $E_D$  is the equivalent Young's modulus of the RVE with damage. According to Eq. (1), the constitutive relation of the damaged material can be written as follows:

$$\varepsilon_{ij} = \frac{1 + \nu}{E} \frac{\sigma_{ij}}{1 - D} - \frac{\nu}{E} \frac{\sigma_{kk} \delta_{ij}}{1 - D}, \quad (2)$$

where  $\sigma_{ij}$ ,  $\varepsilon_{ij}$ , and  $\nu$  are the stress, the strain, and Poisson's ratio, respectively. Under uniaxial loadings, Eq. (2) can be simplified to

$$\sigma = E(1 - D)\varepsilon. \quad (3)$$

Xiao et al.<sup>[17]</sup> proposed a damage evolution model for high cycle fatigue as follows:

$$\frac{dD}{dN} = \alpha \left( \frac{\sigma_a}{1 - n\sigma_m} \right)^m (1 - D)^{-\beta}, \quad (4)$$

where  $\sigma_a$  and  $\sigma_m$  represent the stress amplitude and the mean stress of the fatigue loadings, respectively.  $\alpha$ ,  $\beta$ ,  $m$ , and  $n$  are the material parameters determined by the experimental data of plain fatigue. The damage evolution model can be used to analyze the high cycle fatigue life under uniaxial loadings. However, the stress and strain in the fretting fatigue are multi-axial. Therefore, the above damage evolution model needs to be extended to a three-dimensional (3D) form. The damage equivalent stress<sup>[16]</sup> is introduced here, and is written as follows:

$$\sigma^*(\sigma_{ij}) = \sigma_{eq} \left( \frac{2}{3}(1 + \nu) + 3(1 - 2\nu) \left( \frac{\sigma_H}{\sigma_{eq}} \right)^2 \right)^{1/2}, \quad (5)$$

where  $\sigma_{eq}$  and  $\sigma_H$  are the Mises stress and the hydrostatic stress, respectively. In this study, the amplitude and mean values of the damage equivalent stress are adopted to describe the evolution of the damage variable, instead of the stress amplitude  $\sigma_a$  and the mean stress  $\sigma_m$  in Eq. (4). The direct subtraction between the maximum and minimum values of the damage equivalent stress in a fatigue loading cycle cannot be used to obtain the amplitude of the damage equivalent stress, since the subtraction result will be zero for some specified multi-axial loading cases. Therefore, the amplitude and the mean value of the damage equivalent stress are represented by two functions of the calculations of the stress components during a fatigue loading cycle, i.e.,

$$\begin{cases} \sigma_a^* = \frac{1}{2} \sigma^*(\sigma_{ij,\max} - \sigma_{ij,\min}), \\ \sigma_m^* = \frac{1}{2} \sigma^*(\sigma_{ij,\max} + \sigma_{ij,\min}), \end{cases} \quad (6)$$

where  $\sigma_{ij,\max}$  and  $\sigma_{ij,\min}$  are the maximum and minimum values of the stress tensor  $ij$  components during one loading cycle.  $\sigma^*(\sigma_{ij,\max} - \sigma_{ij,\min})$  represents the calculation result of Eq. (5) by using the difference between the stress components as its arguments, and  $\sigma^*(\sigma_{ij,\max} + \sigma_{ij,\min})$

represents the calculation result of Eq. (5) by using the sum of the stress components as its arguments. The damage evolution law can be expressed by

$$\frac{dD}{dN} = \alpha \left( \frac{\sigma_a^*}{1 - n\sigma_m^*} \right)^m (1 - D)^{-\beta}, \quad (7)$$

where  $\alpha$ ,  $\beta$ ,  $m$ , and  $n$  are the material parameters identified from the plain fatigue test data. It is worth mentioning that Eq. (6) can be simplified into the form of Eq. (3) in the case of uniaxial fatigue loadings. The identification parameter method will be presented in Subsection 3.2.

### 2.1.2 Location of initial crack

Based on the approach proposed by Hojjati-Talemi and Abdel-Wahab<sup>[9]</sup>, where the maximum damage equivalent stress  $\sigma_{\max}^*$  is used along the contact surface, two modified approaches are developed to predict the location of the initial crack, where both the stress state when the axial loading is at its peak value during a loading cycle and the stress state when the axial loading is at its valley value are considered.

One method is based on the value of the variable  $\sigma_a^*$  defined in Eq. (7), considering two cases of the loading condition in a loading cycle. It is assumed that the location of the initial crack is at the site of the maximum value of  $\sigma_a^*$ , which depends on the values of  $\sigma_{ij,\max}$  and  $\sigma_{ij,\min}$  obtained by the FEA. The other method indicates the location of the initial crack according to

$$\sigma_a^*/(1 - n\sigma_m^*),$$

a part of the function in Eq. (7). The parameter  $n$  needs to be known before the prediction of the initial crack. The results of these approaches are compared in this study.

## 2.2 Critical plane SWT model

For the purpose of comparison, the critical plane model, incorporating the SWT parameter  $S_{\text{wt}}$ <sup>[4-5]</sup>, is adopted for the prediction of the location of the crack initiation and fretting fatigue life. The critical plane models are developed from a physical interpretation of the fatigue process, while the cracks are observed to appear and grow on the certain preferential material plane. The SWT parameter  $S_{\text{wt}}$  assumes that crack initiation occurs on a plane where the product of the maximum normal stress  $\sigma_{\max}$  and the normal strain amplitude  $\varepsilon_a$  are the maximum. It can be expressed as follows:

$$S_{\text{wt}} = \sigma_{\max} \varepsilon_a. \quad (8)$$

The SWT life prediction equation employs the mixed form of the high cycle fatigue equation (the Basquin law) and the low cycle fatigue equation (the Coffin-Manson law), considering the peak stress with the mean stress effect, i.e.,

$$S_{\text{wt}} = \sigma_{\max} \varepsilon_a = \frac{(\sigma'_f)^2}{E} (2N_f)^{2b} + \sigma'_f \varepsilon'_f (2N_f)^{b+c}, \quad (9)$$

where  $\sigma'_f$  and  $b$  are the fatigue strength coefficient and exponent, respectively,  $\varepsilon'_f$  and  $c$  are the fatigue ductility coefficient and exponent, respectively,  $E$  is Young's modulus, and  $N_f$  is the number of the fatigue cycles to the crack initiation.

The critical plane SWT parameter is calculated at the integration points of elements by transforming the stress and strain data onto the planes at  $3^\circ$  intervals over a  $180^\circ$  range. The maximum normal stress  $\sigma_{\max}$  and the corresponding normal strain amplitude  $\varepsilon_a$  are determined for each of the 60 planes at each integration point. Therefore, the maximum SWT values are obtained at each integration point, and the number of the failure cycles can be obtained from Eq. (9).

The material parameters of the critical plane SWT model used in this paper are from Ref. [8], and are listed in Table 1.

**Table 1** Material parameters of critical plane SWT model for Ti-6Al-4V

$\sigma'_f$	$b$	$\varepsilon'_f$	$c$
2 500	-0.108	0.841	-0.688

### 2.3 Energy wear model

The energy wear model considers the interfacial shear work as the significant wear parameter controlling the wear volume calculation, which can be expressed by

$$V = \phi \Sigma W, \quad (10)$$

where  $\phi$  is the wear coefficient, and  $\Sigma W$  is the accumulated dissipated energy. For a 2D fretting model, at the time  $t$  and the position  $x$  along the contact surface, the local wear depth can be expressed by<sup>[13]</sup>

$$h(x, t) = \phi \int_0^t q(x, t) ds(x, t), \quad (11)$$

where  $q(x, t)$  is the local shear traction, and  $ds(x, t)$  is the increment of the local relative slip.

Fridrici et al.<sup>[18]</sup> have studied the fretting wear of Ti-6Al-4V by use of the energy wear model with the wear coefficient value of  $2.9 \times 10^{-8} \text{ MPa}^{-1}$ . With the consideration of the material mechanical constants and fretting loading conditions in this study, the same value of the wear coefficient is chosen here. The appropriateness of this value will be validated by the wear analysis and fatigue life prediction.

## 3 Material and FE models

### 3.1 Material

The experimental data from Jin and Mall<sup>[19]</sup> are used to validate the approach developed in this research. The material used in the experiments is Ti-6Al-4V<sup>[20]</sup>, which is commonly used in aerospace structures because of its low density and good mechanical properties. Two cylindrical pads on the flat specimen contact configuration are used in the experiments (see Fig. 1). A dog-bone type of specimen is adopted, and the width and thickness of the reduced area are 6.4 mm and 3.8 mm, respectively. The cylindrical pads are made of Ti-6Al-4V, and their radius is 5.08 cm (see Fig. 2). When the test goes on, the normal pressure force on each fretting pad is 1334 N, the stress ratio is 0.03, and the frequency on the specimen is 2 Hz. The details on the test setup are described in Refs. [20] and [21]. The elastic modulus of the material is 126 GPa, and the yield strength and Poisson's ratio of the material are 930 MPa and 0.3, respectively.

### 3.2 Material parameters for continuum damage model

One advantage of the continuum damage model presented in this study is that the material parameters can be obtained according to the plain fatigue experimental data, instead of the fretting fatigue experimental data. The parameters are obtained from the plain fatigue experimental data obtained in Ref. [22]. Two types of specimens made of Ti-6Al-4V, i.e., unnotched and notched, are analyzed experimentally at the different stress ratios, i.e.,  $R = -0.5$  and  $R = 0.1$ .

In the case of uniaxial loadings, the variables  $\sigma_a^*$  and  $\sigma_m^*$  are equal to the stress amplitude  $\sigma_a$  and the mean stress  $\sigma_m$ , respectively. The number of the cycles to failure  $N_f$  under the constant amplitude loading can be obtained by integrating Eq. (4) from  $D = 0$  (the initial undamaged state) to  $D = 1$  (the macro-crack initiation) as follows:

$$N_f = \frac{1}{\alpha(1 + \beta)} \left( \frac{\sigma_a}{1 - n\sigma_m} \right)^{-m}. \quad (12)$$

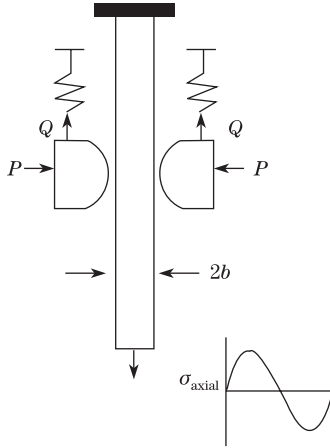


**Fig. 1** Schematic view of fretting fatigue test setup<sup>[5]</sup>

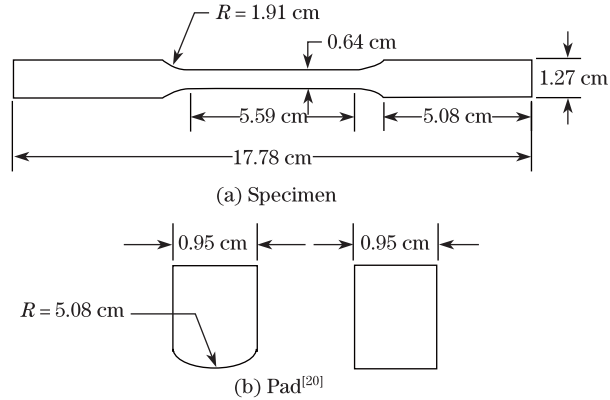


**Fig. 2** Schematic drawing of specimen and pad<sup>[20]</sup>

The experimental data<sup>[22]</sup> at the stress ratios  $R = -0.5$  and  $R = 0.1$  are adopted to determine the four material parameters in Eq. (12). First, the parameters  $m$ ,  $n$ , and  $1/(\alpha(1 + \beta))$  can be obtained from two groups of unnotched specimen experimental data. Then, the independent parameters  $\alpha$  and  $\beta$  will be identified from one group of fatigue test data in the notched specimens by the numerical method introduced by Zhang et al.<sup>[8]</sup>. The fatigue test data of the notched specimens under the stress ratio of  $R = -0.5$  are chosen. Finally, the material parameters for the Ti-6Al-4V used in this study are listed in Table 2.

**Table 2** Material parameters of continuum damage fatigue model for Ti-6Al-4V

$\alpha$	$\beta$	$m$	$n$
$3.00578 \times 10^{-35}$	8.0	10.0818	0.00093248

### 3.3 FE models

A two-dimensional (2D) FE model is developed, including one cylindrical pad and a half of the specimen due to the symmetry along the axial centerline of the specimen. The length and width of the specimen are 15 mm and 6.4 mm, respectively. For the purpose of illustrating the effects of the specimen thickness on the stress state and the fretting fatigue life, two models with different specimen thicknesses are studied, i.e., 15 mm and 1.9 mm. The FE models, including the detailed mesh in the contact zone, are illustrated in Fig. 3. A modified modeling approach developed by Hojjati-Talemi and Abdel-Wahab<sup>[9]</sup> is adopted in this study, where the main feature is the form of the displacement constraint on the FE model. The specimen is restricted from the vertical movement along its bottom surface but free to roll in the  $x$ -direction and along its bottom edge. Both sides of the cylindrical pad are restricted to move just in the vertical direction. The advantage of this modeling approach is that it is convenient to exert the axial stress  $\sigma_{axial}$  and the tangential force  $Q$  on the model.

The non-linear and FE code ABAQUS is used here. The Python code is used for the automatic preprocessing purpose. A 4-node (bilinear) plane strain quadrilateral element (CPE4) is used in the present study. The contact between the fretting pad and the specimen is defined by use of the master-slave algorithm for the contact between the surfaces. Parts of the top specimen surface are defined as the master surface, and parts of the circular surface of the pad are defined as the slave surface. The contact parameters ADJUST and FINITE SLIDING are used. The coulomb friction is used based on the Lagrange multiplier contact algorithm

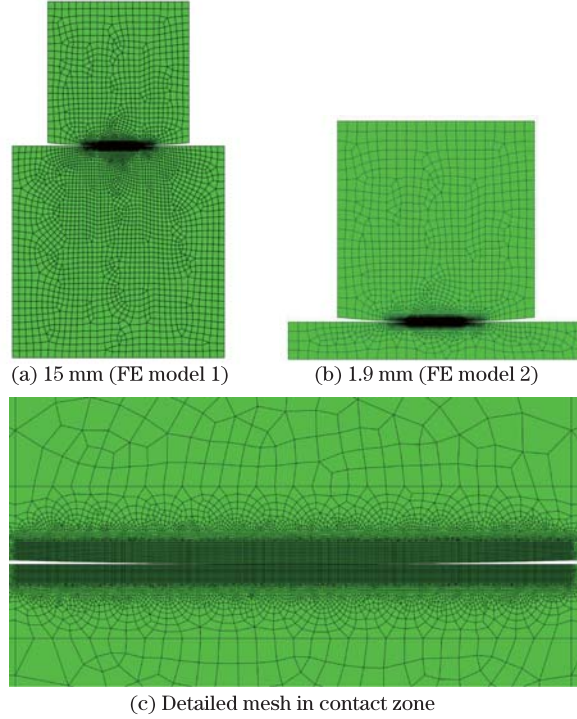


**Fig. 3** FE models with specimen thickness

to ensure the exact stick condition when the shear stress is less than the critical shear value according to the Coulomb friction law. The constant friction coefficient  $\mu = 0.6$  is considered throughout the analysis<sup>[19]</sup>. The element length and width on the contact surface are  $5 \mu\text{m}$ , and gradually increase in the region away from the contact zone (see Fig. 3(c)).

The loadings are used in three steps. The normal pressure load  $P$  is exerted in the first two steps, and remains constant in the third step by the adoption of the multi-point constraint (MPC)<sup>[9]</sup>. In the first step, the normal pressure load with a unit value is applied on the top surface of the pad to establish the contact between the pad and specimen more easily, and the value will be increased to the experimental value in the second step. The axial stress is used at the right-side of the specimen in the third step. The tangential force, which is in the phase with the axial stress, is defined by subtracting the reaction stress used on the left-side of the specimen from the axial stress. The experimental data of the tangential force are used to calculate the reaction stress.

$$\sigma_R = \sigma_{\text{axial}} - Q/A_s, \quad (13)$$

where  $\sigma_R$  is the reaction stress on the left-side of the specimen,  $\sigma_{\text{axial}}$  is the axial stress, and  $A_s$  represents the cross-sectional area of the specimen. Figure 4 shows the schematic of the fretting loading history. Because there is no restriction of horizon movement on the specimen, it is necessary to ensure that  $Q < \mu P$ . Therefore, the contact remains in a partial slip.

### 3.4 Verification of FE models

A mesh convergence study is conducted to validate the appropriateness of the current mesh size at the contact region between the pad and the specimen. The two models with different specimen thicknesses mentioned above are analyzed, and the numerical results are compared with the analytical results reported by Nowell and Hills<sup>[1]</sup>.

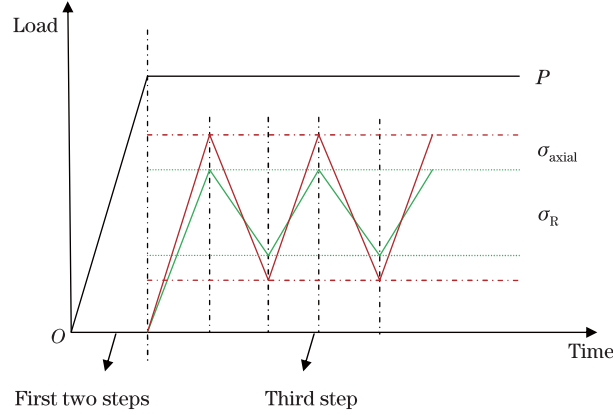


**Fig. 4** Schematic of fretting loading history

Based on the Hertzian contact theory<sup>[23]</sup>, the half width of the contact zone  $a$  will be  $440 \mu\text{m}$ , and the half space assumption is considered to be met if the specimen thickness  $d$  is at least 10 times or more than the semi-contact width<sup>[9]</sup>, or in other words,  $d/a > 10$ . The specimen thickness in Fig. 3(a) is  $15 \text{ mm}$  and the value of  $d/a$  for this model is about 34. But for the case shown in Fig. 3(b), the value of  $d/a$  is about 4.3, and the half space assumption is violated, which results in significant deviation from the analytical solution.

For the sake of simplicity, the loading condition for the verification is specified to

$$P = 1334 \text{ N}, \quad \sigma_{\text{axial}} = 100 \text{ MPa}, \quad Q = 400 \text{ N},$$

which makes sure that there are closed forms for the equations in the solution obtained in Ref. [1]. The frictional shear stress  $q(x)$  along the contact surface and the stress in the  $x$ -direction along the contact surface  $\sigma_{xx}$  are chosen to validate the mesh. Under the specified loading, the equation<sup>[1]</sup>

$$\frac{\sigma_{\text{axial}}}{\mu p_0} \leq 4 \left( 1 - \sqrt{1 - \frac{Q}{\mu P}} \right) \quad (14)$$

is met so that the closed forms for the equations of the variables  $q(x)$  and  $\sigma_{xx}$  exist, where  $p_0$  is the maximum Hertzian pressure. Figures 5(a) and 5(b) depict the normalized frictional shear stress  $q(x)/(\mu p_0)$  and the normalized stress in the  $x$ -direction  $\sigma_{xx}/(\mu p_0)$  along the contact surface for the analytical solution and the two numerical results. The numerical results of the specimen model with the thickness of  $15 \text{ mm}$  are closer to the analytical solution. The difference of  $\sigma_{xx}/(\mu p_0)$  between the two numerical results reaches 10.2% at the right edge of the contact.

## 4 Computational method

The approach involves the simulation of the damage-coupled constitutive model, the damage evolution model, and the energy wear model. The constitutive model and damage evolution model are implemented through the user subroutine UMAT in ABAQUS. During each loading cycle, the UMAT subroutine is used to calculate the stress and strain for the damaged material and the damage increment at each integration point. Since it is computationally expensive to simulate each loading cycle, the jump-in-cycle procedure is adopted in the numerical implementation, which assumes that the stress and damage remain unchanged for a finite period of

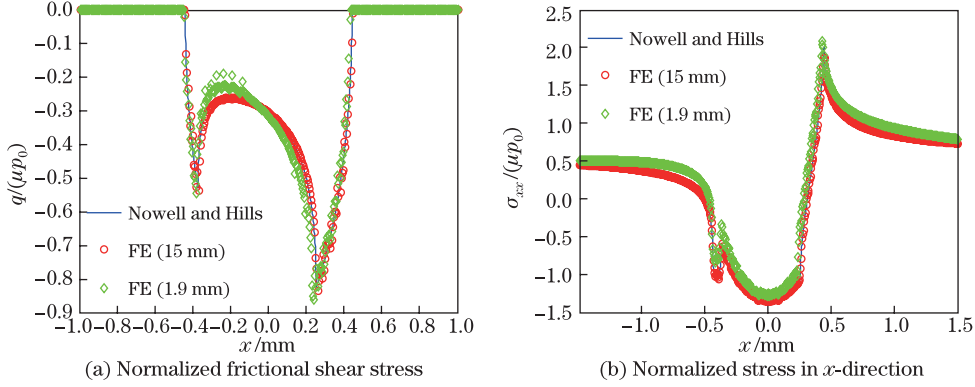


**Fig. 5** Comparison of normalized frictional shear stress and normalized stress in  $x$ -direction obtained in Ref. [1] and two FE numerical results with different thicknesses

$\Delta N$  cycles, constituting a block. Then, the damage evolution can be interpreted as piecewise linear with respect to the number of the cycles. It is necessary to note that the value of  $\Delta N$  is determined to obtain a convergent fretting fatigue life.

The energy wear model is implemented in the FE code ABAQUS through the user subroutine UMESHMOTION. The adaptive meshing user subroutine is called after the equilibrium iteration of each time increment to simulate the material removal is reached. The jump-in-cycle procedure is also employed.

The whole algorithm is illustrated in the flowchart of Fig.6, and the detailed steps of the numerical implementation are listed as follows.

- (i) The initial damage for each element is assumed to be zero.
- (ii) The stress field and related contact variables are calculated for each block by the given UMAT subroutine.
- (iii) If the wear effect is considered during each block, three steps to implement the wear model are listed as follows; otherwise this step can be ignored.
  - (iii-1) For a contact node, the increment of the local wear depth at the  $k$ th time increment for a block can be written as

$$\Delta h = \phi \Delta N q_k \Delta s_k, \quad (15)$$

where  $q_k$  and  $\Delta s_k$  are the shear traction and the incremental slip at the  $k$ th time increment, respectively. The increment of the local wear depth  $\Delta h$  is implemented by moving the surface nodes in the local normal direction at the end of each time increment. This geometry update is implemented as a purely Eulerian analysis.

(iii-2) The material variables are re-mapped to the new position by the advection from the old location to the new location by solving the advection equations with a second-order numerical method called the Lax-Wendroff method<sup>[24]</sup>.

(iii-3) Repeat (iii-1) and (iii-2) until the number of the time increment  $k$  reaches the maximum number of the time increments within one fretting cycle  $M_{\max}$ . In this study,  $M_{\max} = 40$ .

(iv) After each block, the damage evolution rate is calculated according to the stress field and Eq. (7). The damage values and the number of the cycles for all elements are updated at the end of the current block.

$$D_j^{i+1} = D_j^i + \left( \frac{dD}{dN} \right)_j^i \Delta N, \quad (16)$$

$$N^{i+1} = N^i + \Delta N, \quad (17)$$

where  $i$  represents the current block, and  $j$  is the number of the elements. Then, the material properties can be modified based on the calculated damage value for the next block such as the equivalent Young's modulus of the RVE with damage.

(v) The algorithm repeats (ii)–(iv) for each block of cycles until the accumulated damage of any integration point reaches the critical value  $D_c$ . The number of the cycles at this stage is the fretting fatigue crack initiation life. In this study, the critical value is set to be 1.

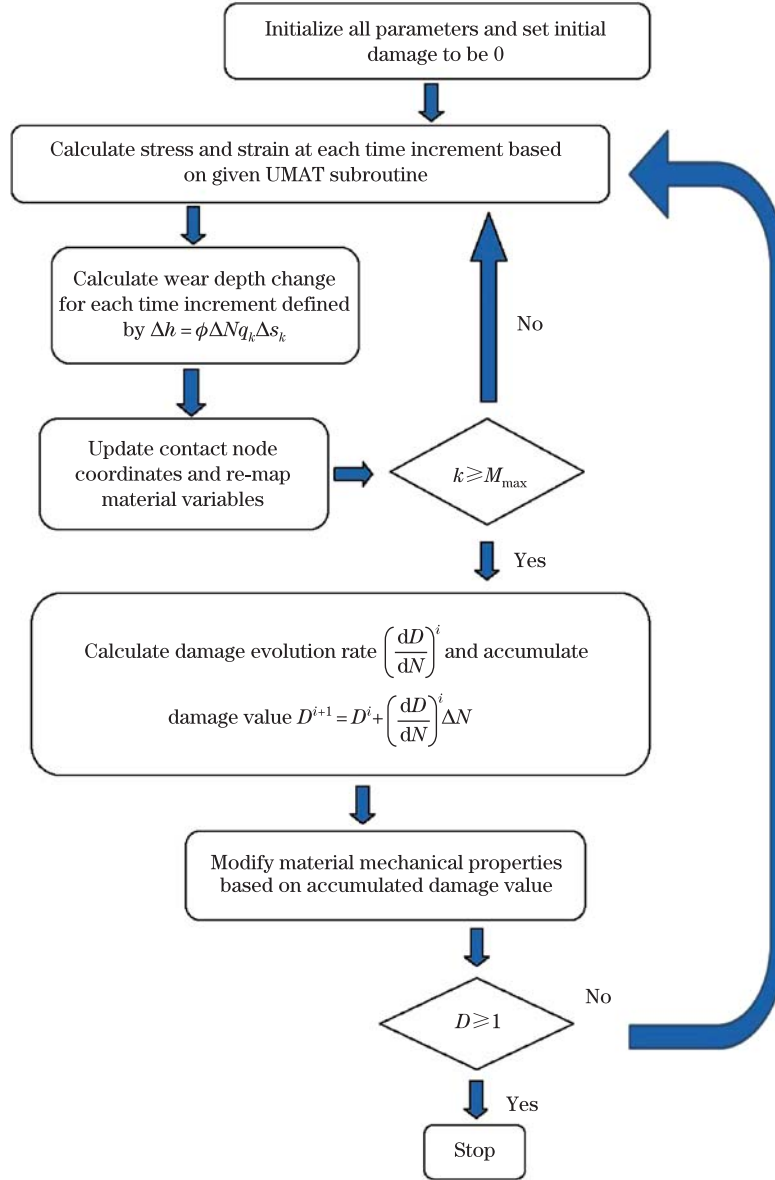


Fig. 6 Flowchart of algorithm at each integration point

## 5 Results and discussion

The two main contact states, i.e., the partial slip and the gross slip, exist in the fretting problem. In the partial slip regime, the contact zone can be divided into an external slip zone

and an internal stick zone. In the gross slip regime, the entire contact zone is the slip zone. However, it is found that wear still exists in the partial slip case based on the experimental studies of Jin and Mall<sup>[20–21]</sup>, Ding et al.<sup>[25]</sup>, and Mohd-Tobi et al.<sup>[26]</sup>, which is less severe than that in the gross sliding case.

In this study, the tangential force  $Q$  instead of the applied pad displacement  $\Delta d_{\text{app}}$  in the experiments<sup>[19]</sup> is used to conduct the FEA and subsequently predict the fretting fatigue life. Based on the configuration of the FE models, it is necessary to make sure that contact remains in the partial slip condition. In other words,

$$Q < \mu P.$$

The four tests mentioned in Ref. [19] (see Table 3) are analyzed by the continuum damage mechanics (CDM) approach. Two FE models with different specimen thicknesses are examined for each test to reveal the effects of the thickness. The detailed procedures of the analyses are listed as follows.

First, the wear effect is ignored, and all the four tests with two different specimen thicknesses are calculated by the CDM approach and the critical plane SWT method for the comparison.

Secondly, the wear effect is considered in the case of the model with the specimen thickness of 1.9 mm by the CDM approach.

**Table 3** Experimental data of four tests chosen from Ref. [19]

Test	$S_a/\text{MPa}$	$\Delta d_{\text{app}}$	$Q_{\text{max}}/N$	$Q_{\text{min}}/N$	$Q_{\text{max}}/P$	Contact condition	$N_f$
1	267	0	552	−458	0.41	Partial slip	$1.19 \times 10^5$
2	290	0	756	−450	0.56	Partial slip	$8.91 \times 10^4$
3	315	0	712	−533	0.53	Partial slip	$5.15 \times 10^4$
4	242	0	512	−409	0.38	Partial slip	$1.66 \times 10^5$

The results, including the location of the initial crack and the fretting fatigue life, are compared with the experimental data. It is noted that the stress in the unworn case is used to calculate the fretting fatigue life in the critical plane SWT method.

## 5.1 Prediction for location of initial crack

### 5.1.1 Without wear effect

Five methods are used to predict the location of the initial crack, three of which are based on the continuum damage mechanics by use of the variables  $\sigma_{\text{max}}^*$ ,  $\sigma_a^*$ , and  $\sigma_a^*/(1 - n\sigma_m^*)$ , respectively. These three variables are defined in Subsection 2.1.2, and can be calculated conveniently according to the stress state along the contact surface. The fourth method is the critical plane SWT method. The fifth method is the CDM approach. With these methods, the location of the initial crack can be found at the position where the damage value reaches 1. Tables 4 and 5 show the results of the location of the initial crack predicted for FE model 1 and FE model 2, respectively. All the five results are very close to each other, and are near the right edge of contact.

Figure 7 shows the distribution of the damage mechanics variables and the critical plane SWT parameter at the contact interface for FE model 2 in the case of Test 1. When the thickness of the FE model changes from 15 mm to 1.9 mm, the location of the initial crack shifts towards the center of the contact zone (see Tables 4 and 5).

### 5.1.2 With wear effect

A significant variation of the results is found when the wear effect is considered (see Table 5). The contact geometry of the surfaces gradually changes due to the wear, which results in the evolution of the contact stresses. Figure 8 shows the evolution of the wear scar along the contact surface on the specimen for FE model 2 in the case of Test 2. Wear only occurs at the

external slip zones, and no wear scar exists at the central stick zone. The wear scar at the right slip zone is significant compared with that at the left slip zone. It approaches a punch on the flat contact. The original critical position for the crack initiation near the right contact edge is worn away (see Fig. 8). The right stick-slip interface between the stick and the slip zone is a critical position, which is extremely close to the initiation site of the crack (see Fig. 8). Similar results were also reported by Madge et al.<sup>[27–28]</sup>.

**Table 4** Predicted location of initial crack ( $x/a$ ) for FE model 1

Test	$\sigma^*$	$\sigma_a^*$	$\sigma_a^*/(1 - n\sigma_m^*)$	SWT	CDM without wear
1	0.974 4	0.963 1	0.974 4	0.974 4	0.974 4
2	0.963 1	0.963 1	0.963 1	0.974 4	0.974 4
3	0.963 1	0.963 1	0.963 1	0.974 4	0.974 4
4	0.974 4	0.974 4	0.974 4	0.974 4	0.940 4

**Table 5** Predicted location of initial crack ( $x/a$ ) for FE model 2

Test	$\sigma^*$	$\sigma_a^*$	$\sigma_a^*/(1 - n\sigma_m^*)$	SWT	CDM without wear	CDM with wear
1	0.940 4	0.940 4	0.940 4	0.940 4	0.940 4	0.284
2	0.929 1	0.940 4	0.929 1	0.940 4	0.940 4	0.170
3	0.929 1	0.940 4	0.929 1	0.940 4	0.940 4	0.170
4	0.940 4	0.940 4	0.940 4	0.951 8	0.940 4	0.352

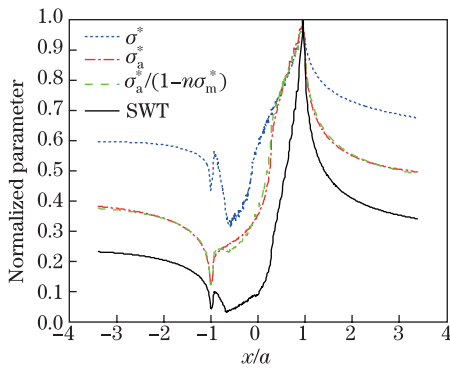


**Fig. 7** Distribution of damage mechanics variables and critical plane SWT parameter at contact interface for FE model 2 in case of Test 1

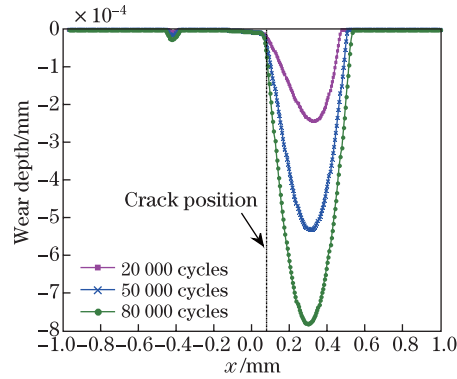


**Fig. 8** Evolution of wear scar along contact surface on specimen for FE model 2 in case of Test 2

## 5.2 Prediction for fretting fatigue life

### 5.2.1 Without wear effect

Figure 9(a) shows the fretting fatigue damage contour of parts of the specimen when the initial crack occurs for FE model 2 of Test 1. The maximum value of the damage value at the nodes in Fig. 9(a) is less than 1. This is because that the algorithm does not record the calculated results when the maximum value of damage exceeds 1. The damage localizes at a very small zone of the contact interface.

For the case of the specimen with the thickness of 1.9 mm, since the stress is higher than that of the specimen with the thickness of 15 mm, the fatigue lives predicted by the CDM

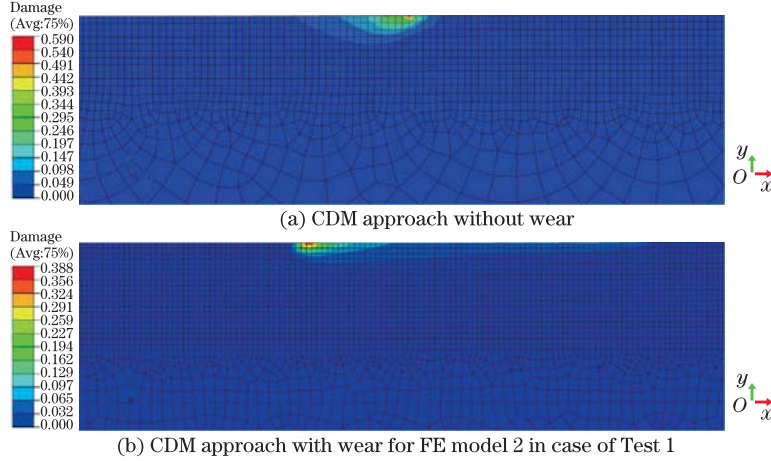


**Fig. 9** Fretting fatigue damage contour for FE model 2 in case of Test 1

approach and the critical plane SWT method are both shorter. The results are listed in Table 6. Figure 10 shows the comparison of the experimental results and the predicted results. The results from the critical plane SWT method are almost the same when the specimen thickness changes. However, the specimen thickness has a significant effect on the results obtained from the CDM approach. All the results for FE model 2 estimated by the CDM method fall within the factor of three scatter bands.

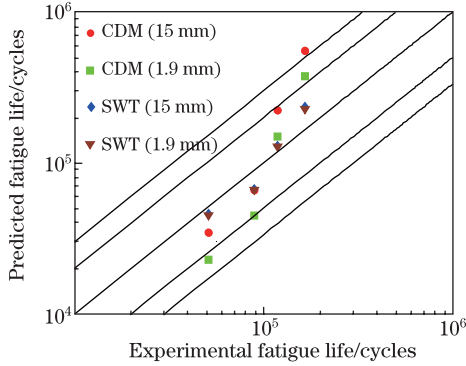
**Table 6** Comparison of experimental and predicted fretting fatigue lives

Test	$N_f$	FE model 1		FE model 2		
		SWT	CDM without wear	SWT	CDM without wear	CDM with wear
1	$1.19 \times 10^5$	$1.30 \times 10^5$	$2.23 \times 10^5$	$1.28 \times 10^5$	$1.50 \times 10^5$	$1.01 \times 10^5$
2	$8.91 \times 10^4$	$6.67 \times 10^4$	$6.64 \times 10^4$	$6.59 \times 10^4$	$4.48 \times 10^4$	$8.60 \times 10^4$
3	$5.15 \times 10^4$	$4.57 \times 10^4$	$3.44 \times 10^4$	$4.47 \times 10^4$	$2.29 \times 10^4$	$8.40 \times 10^4$
4	$1.66 \times 10^5$	$2.34 \times 10^5$	$5.54 \times 10^5$	$2.26 \times 10^5$	$3.75 \times 10^5$	$1.20 \times 10^5$

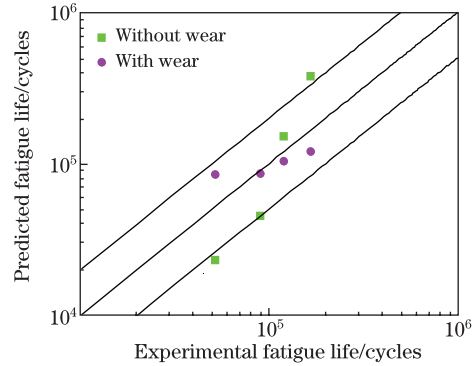
### 5.2.2 With wear effect

Figure 9(b) shows the fretting fatigue damage contour of parts of the specimen when the wear effect is considered. Due to the wear, the damage zone is wider than that in Fig. 9(a). Figure 11 shows the comparison of the results obtained by the CDM approach without and with wear for FE model 2. Two obvious trends can be found: (I) When the fatigue loadings, including the remote axial stress and the tangential force, are low, such as Tests 1 and 4, the width of the wear scar is small. Figure 12 depicts the evolution of the distribution of the Mises stress along the contact surface for FE model 2 in the case of Test 4. The peak of the Mises stress transfers from the initial right contact edge to the position of the crack. The value of the Mises stress first decreases and then increases when the number of the loading cycles increases. The increased Mises stress leads to a shorter fretting fatigue life than that obtained by the CDM approach without the wear effect. (II) For Tests 2 and 3, the tangential forces are close to the threshold value of the gross slip. The width and depth of the wear scar are both bigger. Figure 13 shows the evolution of the Mises stress along the contact surface for FE model 2 in the case of Test 2. The peak also moves from the initial right contact edge to the position of the crack, but the peak value decreases when the cycles increase. Therefore, the predicted fretting fatigue life obtained by the CDM approach with the wear effect is longer. As shown

in Fig. 11, the CDM approach with the wear effect can give more accurate estimates for the fretting fatigue life.



**Fig. 10** Comparison of experimental and predicted results of different thicknesses by approaches without wear



**Fig. 11** Comparison of results of 1.9 mm thickness obtained by CDM approach without and with wear for FE model 2

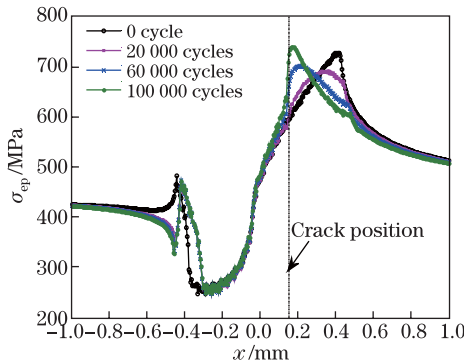


**Fig. 12** Evolution of distribution of Mises stress along contact surface for FE model 2 in case of Test 4

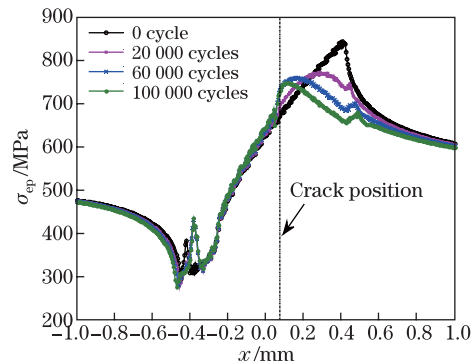


**Fig. 13** Evolution of distribution of Mises stress along contact surface for FE model 2 in case of Test 2

## 6 Conclusions

The focus of this study is to develop a CDM approach to the fretting fatigue crack initiation life prediction. A new fatigue damage model based on the theory of continuum damage mechanics is proposed for the analysis of a multi-axial fatigue problem. On the basis of this model, the damage evolution parameters of the material are obtained in a simple way by use of the experimental data of plain fatigue tests. The wear effect is considered in the CDM approach by implementing the energy wear law to simulate the evolution of the contact geometry. The fretting fatigue life is predicted by the iterated operation on the ABAQUS platform, considering the coupling relation between the stress field and the damage field. The approach is validated with the experimental data obtained from the literature, and is compared with the critical plane SWT method. The following conclusions can be drawn:

(i) For the fretting fatigue under partial slip, the continuum damage mechanics model developed in this study is a good approach, through which the crack initiation site and fretting

fatigue life can be predicted well.

(ii) When the wear effect is ignored, the locations of the initial crack predicted by the CDM approach and critical plane SWT method are very close, and are near the right edge of the contact. After the wear effect is considered, the right stick-slip interface is the position of the crack.

(iii) The CDM approach with the wear effect can give more accurate estimates for the fretting fatigue life.

(iv) The specimen thickness of the FE model can affect the predicted results of the initial crack site and fretting fatigue life. The model with the real specimen thickness is recommended.

(v) Through the FE implementation based on the continuum damage fatigue model, the local damage evolution process can be presented clearly, which is significant for the comprehension on the process of fretting failure.

## References

- [1] Hills, D. A. and Nowell, D. *Mechanics of Fretting Fatigue*, Kluwer Academic Publishers, Dordrecht, 1–14 (1994)
- [2] Nowell, D., Dini, D., and Hills, D. A. Recent developments in the understanding of fretting fatigue. *Engineering Fracture Mechanics*, **73**, 207–222 (2006)
- [3] Nishioka, K. and Hirakawa, K. Fundamental investigations of fretting fatigue: part 6, effects of contact pressure and hardness of materials. *Bulletin of the JSME*, **15**, 135–144 (1972)
- [4] Szolwinski, M. P. and Farris, T. N. Mechanics of fretting crack formation. *Wear*, **198**, 93–107 (1996)
- [5] Lykins, C. D., Mall, S., and Jain, V. An evaluation of parameters for predicting fretting fatigue crack initiation. *International Journal of Fatigue*, **22**, 703–716 (2000)
- [6] Araujo, J. A. and Nowell, D. The effect of rapidly varying contact stress fields on fretting fatigue. *International Journal of Fatigue*, **24**, 763–775 (2002)
- [7] Naboulsi, S. and Mall, S. Fretting fatigue crack initiation behavior using process approach and finite element analysis. *Tribology International*, **36**, 121–131 (2003)
- [8] Zhang, T., McHugh, P. E., and Leen, S. B. Finite element implementation of multiaxial continuum damage mechanics for plain and fretting fatigue. *International Journal of Fatigue*, **44**, 260–272 (2012)
- [9] Hojjati-Talemi, R. and Abdel-Wahab, M. Fretting fatigue crack initiation lifetime predictor: using damage mechanics approach. *Tribology International*, **60**, 176–186 (2013)
- [10] McColl, I. R., Ding, J., and Leen, S. B. Finite element simulation and experimental validation of fretting wear. *Wear*, **256**, 1114–1127 (2004)
- [11] Madge, J. J., Leen, S. B., and Shipway, P. H. The critical role of fretting wear in the analysis of fretting fatigue. *Wear*, **263**, 542–551 (2007)
- [12] Madge, J. J., Leen, S. B., McColl, I. R., and Shipway, P. H. Contact-evolution based prediction of fretting fatigue life: effect of slip amplitude. *Wear*, **262**, 1159–1170 (2007)
- [13] Zhang, T., McHugh, P. E., and Leen, S. B. Computational study on the effect of contact geometry on fretting behavior. *Wear*, **271**, 1462–1480 (2011)
- [14] Fouvry, S., Liskiewicz, T., Kapsa, P. H., Hannel, S., and Sauger, E. An energy description of wear mechanisms and its applications to oscillating sliding contacts. *Wear*, **255**, 287–298 (2003)
- [15] Lemaitre, J. and Chaboche, J. L. *Mechanics of Solid Materials*, Cambridge University Press, Cambridge (1990)
- [16] Lemaitre, J. and Rodrigue D. *Engineering Damage Mechanics*, Springer, New York (2005)
- [17] Xiao, Y. C., Li, S., and Gao, Z. T. A continuum damage mechanics model for high cycle fatigue. *International Journal of Fatigue*, **20**, 503–508 (1998)
- [18] Fridrici, V., Fouvry, S., and Kapsa, P. H. Effect of shot peening on the fretting wear of Ti-6Al-4V. *Wear*, **250**, 642–649 (2001)

- [19] Jin, O. and Mall, S. Effects of slip on fretting behavior: experiments and analysis. *Wear*, **256**, 671–684 (2004)
- [20] Jin, O. and Mall, S. Effects of independent pad displacement on fretting fatigue behavior of Ti-6Al-4V. *Wear*, **253**, 585–596 (2002)
- [21] Jin, O. and Mall, S. Influence of contact configuration on fretting fatigue behavior of Ti-6Al-4V under independent pad displacement condition. *International Journal of Fatigue*, **24**, 1243–1253 (2002)
- [22] United States Department of Defense. *Metallic Materials and Elements for Aerospace Vehicle Structures*, United States Department of Defense, New York (1998)
- [23] Johnson, K. L. *Contact Mechanics*, Cambridge University Press, Cambridge (1987)
- [24] Hibbit, Karlsson and Sorensen Inc. *ABAQUS/Standard Version 6.10, User Manual*, Hibbit, Karlsson and Sorensen Inc., Rhode Island (2010)
- [25] Ding, J., Bandak, G., Leen, S. B., Williams, E. J., and Shipway, P. H. Experimental characterization and numerical simulation of contact evolution effect on fretting crack nucleation for Ti-6Al-4V. *Tribology International*, **42**, 1651–1662 (2009)
- [26] Mohd-Tobi, A. L., Ding, J., Bandak, G., Leen, S. B., and Shipway, P. H. A study on the interaction between fretting wear and cyclic plasticity for Ti-6Al-4V. *Wear*, **267**, 270–282 (2009)
- [27] Madge, J. J., Leen, S. B., and Shipway, P. H. The critical role of fretting wear in the analysis of fretting fatigue. *Wear*, **263**, 542–551 (2007)
- [28] Madge, J. J., Leen, S. B., McColl, I. R., and Shipway, P. H. Contact-evolution based prediction of fretting fatigue life: effect of slip amplitude. *Wear*, **262**, 1159–1170 (2007)